

1 **A phylogenomic perspective on the radiation of**
2 **ray-finned fishes based upon targeted sequencing of**
3 **ultraconserved elements**

4 Michael E. Alfaro^{1,2,*}, Brant C. Faircloth^{1,2}, Laurie Sorenson¹, Francesco Santini¹

5 ¹Department of Ecology and Evolutionary Biology, University of California, Los Angeles, CA, USA

6 ²These authors contributed equally to this work

7 * E-mail: michaelalfaro@ucla.edu

8 Summary

9 Ray-finned fishes constitute the dominant radiation of vertebrates with over 30,000 species.
10 Although molecular phylogenetics has begun to disentangle major evolutionary relationships
11 within this vast section of the Tree of Life, there is no widely available approach for effi-
12 ciently collecting phylogenomic data within fishes, leaving much of the enormous potential
13 of massively parallel sequencing technologies for resolving major radiations in ray-finned
14 fishes unrealized. Here, we provide a genomic perspective on longstanding questions regard-
15 ing the diversification of major groups of ray-finned fishes through targeted enrichment of
16 ultraconserved nuclear DNA elements (UCEs) and their flanking sequence. Our workflow
17 efficiently and economically generates data sets that are orders of magnitude larger than
18 those produced by traditional approaches and is well-suited to working with museum speci-
19 mens. Analysis of the UCE data set recovers a well-supported phylogeny at both shallow and
20 deep time-scales that supports a monophyletic relationship between *Amia* and *Lepisosteus*
21 (Holostei) and reveals elopomorphs and then osteoglossomorphs to be the earliest diverging
22 teleost lineages. Divergence time estimation based upon 14 fossil calibrations reveals that
23 crown teleosts appeared 270 Ma at the end of the Permian and that elopomorphs, osteoglos-
24 somorphs, ostarioclupeomorphs, and euteleosts diverged from one another by 205 Ma during
25 the Triassic. Our approach additionally reveals that sequence capture of UCE regions and
26 their flanking sequence offers enormous potential for resolving phylogenetic relationships
27 within ray-finned fishes.

28 Introduction

29 The ray-finned fishes (Actinopterygii) constitute the dominant radiation of vertebrates on
30 the planet including more than 32,000 species and equaling or exceeding richness estimates
31 for the combined total of birds, mammals, and reptiles. Despite a long history of sys-
32 tematic study, resolution of phylogenetic relationships within this vast radiation remains
33 elusive. Studies based upon traditional morphological and single-gene, PCR-based molecu-
34 lar approaches have succeeded in delineating several major lineages of ray-finned fishes, but
35 conflict over how these lineages are related to one another remains. For example, the earliest
36 morphological studies of ray-finned fishes unite gar (*Lepisosteus*) with the bowfin (*Amia*)
37 in the clade Holostei [1, 2] though this clade is not recovered in some later analyses [3, 4].
38 The early branching of teleost lineages has also been historically contentious. Systematists
39 agree on the four earliest-diverging lineages: the osteoglossomorphs (bony-tongues; arawanas,
40 elephant fishes, and allies), the elopomorphs (tarpons, bonefishes, and eels), the ostarioclu-
41 peomorphs (anchovies and herrings, minnows, characins, catfishes, and electric eels), and the
42 euteleosts (salmons, pikes, lizardfishes, and perch-like fishes). However, there is disagreement
43 over both the relationships among these groups and the basal divergences within euteleosts.
44 Recent morphological and molecular studies support a sister-group relationship between os-
45 tarioclupeomorphs and euteleosts [5–7], but beyond this there is little agreement regarding
46 the relationship among these ancient teleost lineages. Morphological analyses alternatively
47 place the osteoglossomorphs [8] or the elopomorphs [5, 9–11] as the sister group to all other
48 teleosts and the remaining lineages sister to the ostarioclupeomorph/euteleost clade. Some
49 molecular analyses place elopomorphs and osteoglossomorphs as the sister group to remain-
50 ing teleosts [12, 13] while others recover a basal divergence between osteoglossomorphs and
51 other teleosts [7, 14].

52 Recently, Near *et al.* [14] used wide-spread taxonomic sampling, in conjunction with se-
53 quence collected from nine commonly used nuclear genes, to provide a more comprehensive
54 phylogenetic hypothesis of relationships among fishes. Their results supported the mono-

55 phyly of the Holostei, suggested that the elopomorphs formed the earliest diverging teleost
56 lineage [15], and provided a new timescale for the divergence of ray-finned fishes. Although
57 promising, these new insights into the radiation of actinopterygians relied upon a relatively
58 modest number of genomic markers, and the stability and timing of these relationship en-
59 coded throughout the genomes of the target groups remain largely untested. One exception
60 to this statement includes a recent study by Zou *et al.* [16] which used transcriptome se-
61 quences to examine basal divergences within euteleosts. However, the Zou *et al.* [16] study
62 did not include several anciently diverging lineages (e.g. *Amia*, osteoglossomorphs) informing
63 questions about the early evolution of major groups of ray-finned fishes.

64 Phylogenomics and next-generation sequencing technologies offer enormous promise for
65 resolving relationships within actinopterygians and other major sections of the Tree of Life.
66 However, revolutions within genomics and informatics have had a surprisingly modest effect
67 on data collection practices within the phylogenetics community: most studies of non-model
68 organisms continue to rely upon direct sequencing of a moderate number of loci, and work-
69 flows that do take advantage of massively parallel sequencing platforms remain bottlenecked
70 by cross-species amplification of phylogenetically informative loci. Several alternatives to
71 traditional phylogenetic workflows exist that help to overcome the inefficiencies of gene-
72 based sequencing. One class of these methods is exemplified by the recent work of Zou *et*
73 *al.* [16], who used a combination of *de novo* transcriptome sequencing, existing transcript
74 data, and computational methods to identify 274 orthologous groups from which they in-
75 ferred the phylogeny of the Actinopterygii. The benefits of their approach include the use of
76 existing, transcript-related data sets (ESTs in GenBank); reasonably well-established data
77 generation methods; and the collection of data from hundreds of loci across the genomes of
78 the focal taxa. Limitations of this approach include reliance on sampling fresh or properly
79 preserved tissues (generally precluding the use of thousands of existing museum samples),
80 dependence of the approach on expression patterns of the tissue sampled, and collection of
81 data from fewer genomic locations than alternative methodologies.

82 A second class of phylogenomic methods involves sequence capture of nuclear regions
83 flanking and including ultraconserved elements (UCEs) [17]. Rather than sequencing ex-
84 pressed portions of the genome, the UCE-based approach involves enriching organismal
85 DNA libraries for hundreds to thousands of UCEs and their flanking regions; sequencing
86 these libraries using massively parallel sequencing; and assembling, aligning, and analyzing
87 the resulting data using informatic tools. This approach has been successfully used in mam-
88 mals [18], birds [17, 19], and reptiles [20] to generate phylogenomic data sets that contain at
89 least one order of magnitude more characters than those generated using PCR and to resolve
90 historically contentious sections of the Tree of Life [18, 20]. The UCE approach differs from
91 transcript-based phylogenomic studies [16] because data collection is independent of expres-
92 sion pattern, researchers can prepare and enrich libraries from existing tissue collections, and
93 UCE loci may be better conserved and more numerous across distantly related taxa [18].

94 Here, we apply the UCE approach to ray-finned fishes by developing a novel set of
95 sequence capture probes targeting almost 500 UCE regions in ray-finned fishes. We use the
96 UCE data to provide the first phylogenomic perspective based upon widespread sampling of
97 hundreds of markers across the genome on long-standing controversies regarding relationships
98 at the base of the ray-finned fish Tree of Life. These include whether *Lepisosteus* and *Amia*
99 form a monophyletic group (the Holostei [1, 2, 21]) and how the major lineages of teleosts,
100 which constitute >99% of ray-finned fishes, are related to one another [5–7, 9–11, 22, 23]. We
101 also use 14 fossil calibrations to provide the first time-scale for ray-finned fishes based upon
102 UCE regions and their flanking sequence. Our results reveal that sequence capture of UCE
103 regions can efficiently and economically generate massive data sets with strong resolving
104 power at both deep and shallow phylogenetic scales within fishes.

105 **Materials and Methods**

106 **Identification of UCE regions**

107 To identify ultraconserved elements (UCEs) in fishes, we used genome-to-genome alignments
108 of stickleback (*Gasterosteus aculeatus*) to medaka (*Oryzias latipes*) to locate nuclear DNA
109 regions of 100% conservation greater than 80 bp in length. To enable efficient capture-probe
110 design, we buffered these regions to 180 bp (where needed) by including equal amounts of
111 medaka sequence 5' and 3' to each UCE. We aligned or re-aligned these buffered regions
112 to the genome-enabled fishes (zebrafish, *Danio rerio*, stickleback, medaka, and two species
113 of puffers, *Tetraodon nigroviridis* and *Takifugu rubripes*) using LASTZ [24], keeping only
114 non-duplicate matches of ≥ 120 bp and $\geq 80\%$ sequence identity across all species in the
115 set. Based on the intersection of UCE loci across all fishes that were greater than 10 Kbp
116 apart, we designed a pilot set of 120 bp sequence capture probes for each of the UCEs
117 present among all members of the set by tiling probes at 4X density. We had these probes
118 commercially synthesized into a custom SureSelect target enrichment kit (Agilent, Inc.). We
119 used a higher than normal [25] tiling density to help ameliorate potential sequence differences
120 among species introduced by buffering shorter UCEs to 180 bp.

121 **Library preparation, UCE enrichment, sequencing, and assembly**

122 We prepared DNA libraries from 18 fish species, including representatives of five acantho-
123 morph orders and two families of perciforms (Table 2), by slightly modifying the Nextera
124 library preparation protocol for solution-based target enrichment [17] and increasing the
125 number of PCR cycles following the tagmentation reaction to 20. Following library prepa-
126 ration, we substituted a blocking mix of 500 μ M (each) oligos composed of the forward and
127 reverse complements of the Nextera adapters for the Agilent-provided adapter blocking mix
128 (Block #3). We incubated species-specific libraries with synthetic RNA probes from the
129 SureSelect kit for 24 h at 65°C. We followed the standard SureSelect protocol to enrich DNA

130 libraries following hybridization; we eluted clean, enriched DNA in 30 μ L of nuclease free
131 water; and we used 15 μ L of enriched template in a 50 μ L PCR reaction of 20 cycles com-
132 bining forward, reverse, and indexing primers with Nextera polymerase to add a custom set
133 of 24 indexing adapters [26]. PCR clean-up was completed using Agencourt AMPure XP.
134 We quantified enriched, indexed libraries using qPCR (Kapa Biosystems), and we prepared
135 two library pools containing 10 libraries at equimolar ratios prior to sequencing.

136 We sequenced each pool of enriched DNA using two lanes of a single-end 100 bp Illu-
137 mina Genome Analyser (GAIIx) run. After sequencing, we trimmed adapter contamination,
138 low quality bases, and sequences containing ambiguous base calls using a pipeline we con-
139 structed (<https://github.com/faircloth-lab/illumiprocessor>). We assembled reads,
140 on a species-by-species basis, into contigs using Velvet [27] and VelvetOptimiser. Follow-
141 ing assembly, we used a software package (<https://github.com/faircloth-lab/phyluce>)
142 containing a custom Python program (match_contigs_to_probes.py) integrating LASTZ [24]
143 to align species-specific contigs to the set of probes/UCEs we used for enrichment while
144 removing reciprocal and non-reciprocal duplicate hits from the data set. During matching,
145 this program creates a relational database of matches to UCE loci by taxon. This pro-
146 gram also has the ability to include UCE loci drawn from existing genome sequences, for
147 the primary purpose of including available data from genome-enabled taxa as outgroups
148 or to extend taxonomic sampling. We used this feature to include UCE loci we identified
149 in the genome sequences of *Gasterosteus aculeatus*, *Haplochromis burtoni*, *Neolamprologus*
150 *brichardi*, *Oreochromis niloticus*, *Oryzias latipes*, *Pundamilia nyererei*, *Takifugu rubripes*,
151 *Tetraodon nigroviridis*, *Gadus morhua*, and *Lepisosteus oculatus*. After generating the rela-
152 tional database of matches to enriched sequences and genome-enabled taxa, we used addi-
153 tional components of PHYLUCÉ (get_match_counts.py) to query the database and generate
154 fasta files for the UCE loci we identified across all taxa. Then, we used a custom python
155 program (seqcap_align_2.py) to align contigs with MAFFT [28] and trim contigs representing
156 UCEs, in parallel, across the selected taxa prior to phylogenetic analysis [17].

157 **Phylogenetic Analyses**

158 The large number of UCE loci we collected create a vast potential space for partitioning data
159 that makes a traditional evaluation of alternative partitioning strategies computationally in-
160 tractable. As a result, we modeled nucleotide substitutions across the concatenated data
161 set using two approaches. For Bayesian analysis, we used a custom script (`run_mraic.py`)
162 wrapping a modified MrAIC 1.4.4 [29] to find the best-fitting model for each UCE locus, we
163 grouped loci having similar substitution models (selected by AICc) into the same partition,
164 and we assigned the partition specific substitution model to all loci concatenated within each
165 partition. For maximum likelihood analyses, we maintained the partitions identified in the
166 Bayesian analysis and we modeled each partition using the GTR+CAT approximation. We
167 performed Bayesian analysis of the concatenated data set using MrBayes 3.1 [30] and two
168 independent runs (4 chains each) of 5,000,000 iterations each, sampling trees every 500 iter-
169 ations, to yield a total of 10,000 trees. We sampled the last 5,000 trees after checking results
170 for convergence by visualizing the log of posterior probability within and between the inde-
171 pendent runs for each analysis, ensuring the average standard deviation of split frequencies
172 was < 0.001 , and ensuring the potential scale reduction factor for estimated parameters was
173 approximately 1.0. We performed maximum likelihood analysis of the concatenated data in
174 RAxML [31] using the rapid bootstrapping algorithm and 500 bootstrap replicates.

175 Gene tree-species tree methods enjoy some advantages over the analysis of concatenated
176 data sets under certain conditions [32–34] but may also be sensitive to missing data [35] and
177 to the resolution of individual gene trees [36]. To minimize the number of unresolved gene
178 tree topologies and maximize the number of topologies that overlapped in sampling the base
179 of the actinopterygian tree, we selected a subset of the UCE contigs containing complete
180 data for *Polypterus* and *Acipenser* and loci ≥ 50 bp, and we used this subset to estimate a
181 species tree with CloudForest (<https://github.com/ngcrawford/CloudForest>), a parallel
182 implementation of a workflow combining substitution model selection (identical to MrAIC
183 1.4.4 [29]) and genetree estimation using PhyML [37]. We estimated the species tree by

184 summarizing gene trees using STAR [38–40]. To assess confidence in the resulting species
185 tree, we used CloudForest to generate 1000, multi-locus, non-parametric bootstrap replicates
186 by resampling nucleotides within loci as well as resampling loci within the data set [41], we
187 summarized bootstrap replicates using STAR, and we reconciled bootstrap replicates with
188 the species tree using RAxML.

189 **Divergence Time Estimation**

190 We used a set of 14 calibration points (Appendix: Fossil calibrations) from previous timetree
191 studies [42, 43] to date several key splits on the tree ranging in age from the Givetian (392
192 Ma) to the early Rupelian (32 Ma). We used the RAxML topology (Fig. 1) plus fossil-
193 derived minimum and maximum age constraints to infer divergence times in BEAST v1.72
194 [44] assuming a GTR model of sequence evolution with gamma-distributed rate variation.
195 Preliminary analyses with the full UCE data (all 491 loci) showed poor mixing under a wide
196 range of fossil constraint parameterizations, and all models incorporating the full UCE data
197 set failed to reach convergence after 300 million generations. To estimate divergence times
198 for these taxa from a large data set, we randomly sampled 50 UCE loci, with replacement, to
199 create five different matrices for BEAST analyses. We analyzed the resulting matrices using
200 independent runs of BEAST. MCMC runs of these data sets mixed much better and showed
201 strong evidence of convergence, having ESS values > 200 for nearly all parameters after 50
202 million generations. However, the parameters for the mean and variance of the lognormally
203 distributed rates mixed much more slowly with autocorrelation times of $\geq 5 \times 10^5$ generations
204 and yielding ESS of $\approx 50 - 100$ across the replicates.

205 **Results and Discussion**

206 **Probe design, UCE enrichment, and sequencing**

207 We located 500 UCEs shared among all actinopterygian fishes, and we designed a set of
208 2,000 capture probes targeting each of these loci (4X coverage). Following enrichment and
209 sequencing, we obtained an average of 2,819,047 reads per species, which we assembled into an
210 average of 665 contigs having an average length of 457 bp (Table 2). After removing contigs
211 that matched no UCEs and UCE loci that matched multiple contigs, we enriched an average
212 of 332 (50%) unique contigs matching UCE loci from each species. Average sequencing depth
213 across UCE loci was 498X. We integrated extant genomic data from several fish species to
214 this group of unique UCE contigs, and we constructed 491 alignments (average length: 305
215 bp, 95 CI: ± 16.0) comprised of 149,246 characters. Each alignment contained an average of
216 21 target taxa (95 CI ± 0.4) after data trimming, and we used this incomplete data matrix
217 for subsequent analyses with RAxML and MrBayes. After removing loci having missing data
218 for *Polypterus* and *Acipenser*, we input 136 alignments (41,731 characters; average length:
219 307 bp, 95 CI: ± 27.7) to CLOUDFOREST for model selection and subsequent species tree
220 estimation using STAR.

221 **A phylogenomic perspective on the basal radiation of ray-finned** 222 **fishes**

223 Maximum likelihood analysis produced a single, completely resolved topology wherein all but
224 two nodes received high (≥ 0.99) bootstrap proportions and Bayesian posterior probabilities
225 (Fig. 1). This topology provides new insight into several long-standing questions concerning
226 the evolution of ray-finned fishes. Our analysis strongly supports the monophyly of the
227 Holostei (*Amia* + *Lepisosteus*). This clade is historically controversial because morphological
228 studies alternatively support [1, 2, 21] and refute [3, 4] the monophyly of this group, while
229 recent molecular studies generally recover the relationship [15, 45, 46]. Additionally, our

230 analyses do not support prior findings of an “ancient fish clade” including the Holostei +
231 Acipenseriformes as the sister group to the teleosts [46, 47]. Rather, our results strongly
232 suggest a traditional relationship in which these lineages form successive sister groups to the
233 teleosts.

234 Our phylogenomic data provide strong evidence for the placement of elopomorphs as
235 the sister group to all other teleosts and osteoglossomorphs and ostarioclupeomorphs as
236 successive sister lineages to the euteleosts (Fig. 1). Our maximum likelihood topology is
237 strongly incongruent with mitogenomic studies [7, 14] but consistent with both a recent
238 analysis of multiple nuclear genes [15] and some of the earliest morphological analyses of
239 the group [5, 9–11]. Within euteleosts, our results are congruent with recent molecular
240 studies [6, 15, 16] in placing esociforms as the sister to salmoniforms rather than any neoteleost
241 lineages.

242 Within acanthomorphs, the largest clade of euteleosts, UCEs recover several intriguing
243 clades that agree with results from recent molecular phylogenetic studies. These include
244 the African cichlids + medaka (Clade C1, Fig. 1), corresponding to an expanded clade of
245 atherinomorphs suggested by recent studies [16, 48, 49]; a clade of gasterosteiforms (stickle-
246 back) and scorpaeniforms (*Taenionotus*) that is congruent with recent molecular and mor-
247 phological studies [16, 50, 51]; and a clade including surgeonfish, frogfishes, and pufferfishes
248 (acanthuroids, lophiiforms, and tetraodontiforms) corresponding to acanthomorph clade “N”
249 of Dettai and Lecointre [15, 52]. Together with the estimated topology, our timetree suggests
250 that UCEs provide sufficient phylogenetic signal to resolve divergences within fishes that are
251 as young as 5 Ma and as old as 400 Ma.

252 The STAR topology was less resolved than topologies based upon analysis of the con-
253 catenated data set (Fig. S1) but recovered largely congruent relationships including a mono-
254 phyletic Holostei as the sister to other actinopterygians, monophyly of elopomorphs, os-
255 teoglossomorphs, ostarioclupeomorphs, and euteleosts, and a successive sister group rela-
256 tionship between ostarioclupeomorphs, *Salvelinus* + *Umbra*, and all remaining euteleosts.

257 The species tree switched the position of the Gadiformes, represented by cod (*Gadus*) and
258 Myctophiformes, represented by *Diaphus*. This resolution is not congruent with results from
259 Near *et al.*, [15] but has been suggested before in other molecular studies [6, 53].

260 **A phylogenomic timescale for the radiation of ancient fish lineages**

261 A general expectation during Bayesian analysis is that runs will converge more quickly on the
262 true posterior distribution with increasing data. However, in our divergence time analysis,
263 we were only able to obtain acceptable mixing in BEAST when analyzing subsamples of
264 the data set; analyses of all 491 loci did not converge despite a diversity of partitioning and
265 calibration strategies combined with long MCMC analyses. This was surprising given the
266 relatively modest number of taxa included in this study and because we fully constrained the
267 topology. Discordant fossil calibrations [54] could potentially underlie poor mixing behavior.
268 However, alternative fossil calibration strategies that enforced subsets of the 14 calibrations
269 revealed that even a single constraint on the age of the root node resulted in analyses with
270 poor mixing behavior. We observed additional evidence that fossil conflict was not the
271 cause of poor mixing because subsampled analyses including all 14 constraints converged
272 and produced nearly identical credible intervals for all nodes (Fig. S2). One possible barrier
273 to good mixing during analyses of the full data set in BEAST may be that the proposal
274 mechanisms and/or tuning parameters for branch lengths are not suited for alignments that
275 contain both very quickly (UCE flanks) and very slowly (UCE core regions) evolving sites.
276 With a large number of sites, even a relatively small change in branch length could result in
277 a large difference in likelihood, resulting in a high rejection rate of branch length proposals.
278 This explanation is consistent with the extremely low acceptance rates we observed in our
279 analyses ($< 5\%$ for branch rate and node height proposals). The recovery of similar age
280 estimates across UCE subsamples (Fig. S2) suggests that the estimated time scale for ray-
281 finned fish diversification adequately reflects the signal for divergences contained within the
282 full UCE data set.

283 Our divergence time analyses suggest that the extant radiation of ray-finned fishes began
284 ≈ 420 Ma near the end of the Silurian. Divergences amongst the actinopteryans, neoptery-
285 gians, and holosteans (Fig. S2, nodes 1-4) are very ancient and span the late Devonian to
286 the early Permian. Extant teleosts (Fig. S2, node 5) can trace their origin back to ≈ 270
287 Ma during the late Permian with primary divergences amongst the elopomorphs, osteoglos-
288 somorphs, ostarioclupeomorphs, and euteleosts occurring before the end of the Triassic. The
289 credible intervals surrounding the age of teleosts are wide, however, and teleosts may have
290 originated as early as 309 Ma during the upper Carboniferous to as late as 226 Ma during
291 the mid-Triassic. We recover a basal split between *Salvelinus* + *Umbra*, representing two
292 protacanthopterygian lineages, and the rest of the euteleosts, at 170 Ma during the Juras-
293 sic (Fig. S2, node 9). Extant acanthomorphs, which comprise the bulk of teleost diversity
294 including over 16,000 species and 300 families, trace their origins to the Cretaceous, ≈ 124
295 Ma (Fig. S2, node 14). We report ages for all splits in Table 1.

296 Our analysis represents the first timescale for ray-finned fishes derived from widespread
297 sampling of the nuclear genome. Previous divergence time analyses based upon fossils, mi-
298 tochondrial DNA, and nuclear DNA have produced conflicting timescales for ray-finned fish
299 diversification. For example, the earliest known fossil teleosts are elopomorphs and ostario-
300 physans, dating to the Late Jurassic [42, 43]. In contrast mitogenomic data consistently sug-
301 gest Paleozoic divergences, usually into the early Permian or late Carboniferous (e.g., [55]).
302 Some divergence time studies based upon nuclear genes have posited Late Triassic to Early
303 Jurassic divergences (173-214 Ma [42, 43]) for the teleosts, while more recent studies that
304 include additional nuclear loci and an improved set of fossil calibrations push the age of
305 crown teleosts to 307 Ma at the end of the Carboniferous [15]. Our UCE-derived date for
306 the divergence of teleosts (≈ 270 Ma) is much older than an earlier estimate based upon
307 *RAG1* sequence [43] and largely overlaps with the age estimate derived by Near et al [15].
308 Other splits within our UCE timescale generally correspond to those derived by Near et
309 al [15] (Fig. S3). One major exception to this observation is divergence of the euteleosts

310 which UCE data estimate to be ≈ 171 Ma (95% credible interval, 152-194 Ma) while tra-
311 ditional nuclear loci estimate an age of ≈ 229 Ma (95% credible interval 220-259 Ma) [15].
312 One possible cause for this difference is age estimates is that we have not sampled some of
313 the earliest diverging euteleost lineages in our study including *Lepidogalaxias*, resulting in an
314 underestimate of the true euteleost crown age. Our molecular timescale provides additional
315 evidence for a relatively ancient origin of teleosts and further highlights the apparent gap in
316 the fossil record between stem and crown members of this clade [15, 42].

317 **Conclusions**

318 Sequence capture of regions anchored by UCEs offers a powerful and efficient means of gener-
319 ating massive genomic data sets capable of resolving phylogenetic relationships at both deep
320 and shallow scales in non-model organisms. Our UCE-based approach offers several advan-
321 tages over previous studies that should contribute to the reliability of our topology. These
322 benefits include efficient sampling of sequence data across individual genomes and among
323 divergent taxa, collection of data from an order of magnitude more loci than studies based
324 upon traditionally-used genetic markers and almost twice as many loci as transcriptome-
325 based genomic studies [16], validity of the UCE probe set across bony fishes spanning 350
326 Ma of evolutionary history, and utility of the UCE enrichment approach with tissues col-
327 lected from museum specimens. Additionally, these data illustrate that biologists can use
328 UCE-based genetic markers to reconstruct the phylogeny of taxa other than amniotes, sup-
329 porting the observation that UCE-based markers are a universal source of phylogenetically
330 informative characters [17, 18].

331 **Acknowledgments**

332 National Science Foundation grants DEB-6861953 and DEB-6701648 (to MEA) and DEB-
333 1242260 (to BCF) provided partial support for this work. Funds from an Amazon Web

334 Services education grant (to BCF) supported computational portions of this work. We
335 thank Bryan Carstens, Scott Herke, and the LSU Genomics Facility for help with Illumina
336 sequencing. We thank Travis Glenn for helpful discussion of several laboratory methods,
337 and we thank John Huelsenbeck, Brian Moore, and John McCormack for helpful discussions
338 relative to phylogenetic analyses. Marc Suchard provided helpful advice about BEAST
339 analyses. Amisha Gadani provided illustrations. We obtained tissues used in this study on
340 loan or as gifts from Peter Wainwright (UC Davis), Rita Metha (UC Santa Cruz), Mark
341 Westneat (Field Museum), Eric Hilton and Patrick McGrath (Virginia Institute of Marine
342 Sciences), David Jacobs and Ryan Ellingson (UCLA), H.J. Walker and Phil Hastings (Scripps
343 Institute of Oceanography), Anindo Choudhury (St. Norbert College).

344 **Author Contributions**

345 MEA, FS, LS, and BCF designed the study. BCF identified conserved regions and designed
346 capture probes. LS and BCF extracted DNA, prepared DNA libraries, and performed DNA
347 sequence enrichments. BCF processed sequence data, assembled sequence data, and created
348 data sets for subsequent analysis. BCF performed gene tree analyses. BCF and MEA
349 performed concatenated analyses. MEA and FS performed dating analyses. MEA, BCF, and
350 FS wrote the manuscript. All authors discussed results and commented on the manuscript.

351 **Data Availability**

352 Contigs assembled from raw read data are available from Genbank (Accession #s: XXX -
353 YYY) **[We are in the process of submitting assembled genomic data to Genbank
354 for archiving, which takes a bit of time given the total amount of data we are
355 submitting]**. Probe data, assembled contigs, alignments, and data sets we used for anal-
356 ysis are temporarily available from [http://fish-phylogenomics.s3-website-us-east-1.
357 amazonaws.com/](http://fish-phylogenomics.s3-website-us-east-1.amazonaws.com/) (we do not log accesses of this website). Upon acceptance of this manuscript,

358 we will make all assembled contigs, capture probes, alignments, and datasets available from
359 Dryad (<http://datadryad.org>). Protocols for library preparation and UCE enrichment
360 are available under Creative Commons license from <http://ultraconserved.org>. Software
361 used for the analysis of raw sequence data are available under BSD-style license from [https:](https://github.com/faircloth-lab/splitaake)
362 [//github.com/faircloth-lab/splitaake](https://github.com/faircloth-lab/splitaake), <https://github.com/faircloth-lab/illumiprocessor>,
363 and <https://github.com/faircloth-lab/phyluce>.

References

- [1] Nelson, G., 1969 Gill arches and the phylogeny of fishes, with notes on the classification of vertebrates. *Bull. Am. Mus. Nat. Hist* **141**, 465–552.
- [2] Jessen, H., 1972 Schultergürtel und pectoralflosse bei actinopterygiern. *Fossils Strata* **1**, 1–101.
- [3] Olsen, P., 1984 The skull and pectoral girdle of the parasemionotid fish *Watsonulus eugnathoides* from the Early Triassic Sakamena Group of Madagascar, with comments on the relationships of the holostean fishes. *J. Vert. Paleontol.* **4**, 481–499.
- [4] Patterson, C., 1973 Interrelationships of holosteans. In *Interrelationships of fishes* (eds. P. Greenwood, R. Miles & C. Patterson), pp. 207–226. London: Academic Press.
- [5] Arratia, G., 2001 The sister-group of Teleostei: Consensus and disagreements. *J. Vert. Paleontol.* **21**, 767–773.
- [6] Li, C., Lu, G. & Orti, G., 2008 Optimal data partitioning and a test case for ray-finned fishes (Actinopterygii) based on ten nuclear loci. *Syst. Biol* **57**, 519.
- [7] Inoue, J. G., Miya, M., Tsukamoto, K. & Nishida, M., 2003 Basal actinopterygian relationships: A mitogenomic perspective on the phylogeny of the "ancient fish". *Mol. Phylogenet. Evol.* **26**, 110–120.
- [8] Patterson, C. & Rosen, D., 1977 Review of ichthyodectiform and other Mesozoic teleost fishes and the theory and practice of classifying fossils. *Bull. Am. Mus. Nat. Hist.* **158**, 83–172.
- [9] Arratia, G., 2010 The clupecocephala re-visited: Analysis of characters and homologies. *Rev. Biol. Mar. Oceanog.* **45**, 635–657.

- 386 [10] Arratia, G., 2004 Mesozoic halecostomes and the early radiation of teleosts. In *Mesozoic*
387 *fishes 3* (eds. G. Arratia & A. Tintori), pp. 279–315. Munich, Germany: Verlag Dr.
388 Friedrich Pfeil.
- 389 [11] Cloutier, R. & Arratia, G., 2004 Early diversification of actinopterygians. In *Recent*
390 *advances in the Origin and Early Radiation of Vertebrates* (eds. G. Arratia, M. V. H.
391 Wilson & R. Cloutier), pp. 217–270. Munich, Germany: Verlag Dr. Friedrich Pfeil.
- 392 [12] Le, H., Lecointre, G. & Perasso, R., 1993 A 28S rRNA-based phylogeny of the gnathos-
393 tomes: First steps in the analysis of conflict and congruence with morphologically based
394 cladograms. *Mol. Phylogenet. Evol.* **2**, 31–51.
- 395 [13] Broughton, R. I., 2010 Phylogeny of teleosts based on mitochondrial genome sequences.
396 In *Origin and Phylogenetic Interrelationships of Teleosts* (eds. J. Nelson, H. Schultz &
397 M. Wilson), pp. 61–76. Munchen: Verlag.
- 398 [14] Inoue, J. G., Miya, M., Venkatesh, B. & Nishida, M., 2005 The mitochondrial genome of
399 Indonesian coelacanth *Latimeria menadoensis* (*Sarcopterygii: Coelacanthiformes*) and
400 divergence time estimation between the two coelacanths. *Gene* **349**, 227–235.
- 401 [15] Near, T. J., Eytan, R. I., Dornburg, A., Kuhn, K. L., Moore, J. A., Davis, M. P.,
402 Wainwright, P. C., Friedman, M. & Smith, W. L., 2012 Resolution of ray-finned fish
403 phylogeny and timing of diversification. *Proc. Natl. Acad. Sci. U.S.A.* **109**, 13698–13703.
- 404 [16] Zou, M., Guo, B., Tao, W., Arratia, G. & He, S., 2012 Integrating multi-origin expres-
405 sion data improves the resolution of deep phylogeny of ray-finned fish (Actinopterygii).
406 *Sci. Rep.* **2**.
- 407 [17] Faircloth, B., McCormack, J., Crawford, N., Harvey, M., Brumfield, R. & Glenn, T.,
408 In Press Ultraconserved elements anchor thousands of genetic markers for target en-
409 richment spanning multiple evolutionary timescales. *Syst. Biol.* (doi:10.1093/sysbio/
410 sys004).

- 411 [18] McCormack, J., Faircloth, B., Crawford, N., Gowaty, P., Brumfield, R. & Glenn, T.,
412 2012 DNA flanking ultraconserved elements provides novel phylogenetic markers and re-
413 solves placental mammal phylogeny when combined with species tree analysis. *Genome*
414 *Res.* **22**, 746–754. (doi:10.1101/gr.125864.111).
- 415 [19] McCormack, J., Harvey, M., Faircloth, B., Crawford, N., Glenn, T. & Brumfield, R.,
416 *In review* A phylogeny of birds based on over 1,500 loci collected by target enrichment
417 and high-throughput sequencing. *PLoS ONE* .
- 418 [20] Crawford, N. G., Faircloth, B. C., McCormack, J. E., Brumfield, R. T., Winker, K.
419 & Glenn, T. C., 2012 More than 1000 ultraconserved elements provide evidence that
420 turtles are the sister group of archosaurs. *Biol. Lett.* **8**, 783–786.
- 421 [21] Grande, L., 2010 An empirical synthetic pattern study of gars (Lepisosteiformes) and
422 closely related species, based mostly on skeletal anatomy: the resurrection of Holostei.
423 *Copeia* pp. 1–863.
- 424 [22] De Pinna, M., 1996 Teleostean monophyly. In *Interrelationships of Fishes* (eds. M. L.
425 Stiassny, L. R. Parenti & G. D. Johnson), pp. 147–162. San Diego: Academic Press.
- 426 [23] Zaragüeta-Bagils, R., Lavoue, S., Tillier, A., Bonillo, C. & Lecointre, G., 2002 As-
427 sessment of otocephalan and protacanthopterygian concepts in the light of multiple
428 molecular phylogenies. *C. R. Biol.* **325**, 1191–1207.
- 429 [24] Harris, R., 2007 *Improved pairwise alignment of genomic DNA*. Ph.D. thesis, The
430 Pennsylvania State University.
- 431 [25] Tewhey, R., Nakano, M., Wang, X., Pabon-Pena, C., Novak, B., Giuffre, A., Lin, E.,
432 Happe, S., Roberts, D., LeProust, E. *et al.*, 2009 Enrichment of sequencing targets from
433 the human genome by solution hybridization. *Genome Biol.* **10**, R116.

- 434 [26] Faircloth, B. C. & Glenn, T. C., 2012 Not all sequence tags are created equal: Designing
435 and validating sequence identification tags robust to indels. *PLoS ONE* **7**, e42543. (doi:
436 10.1371/journal.pone.0042543).
- 437 [27] Zerbino, D. & Birney, E., 2008 Velvet: Algorithms for de novo short read assembly
438 using de Bruijn graphs. *Genome Res.* **18**, 821–829.
- 439 [28] Katoh, K., Kuma, K., Toh, H. & Miyata, T., 2005 MAFFT version 5: Improvement in
440 accuracy of multiple sequence alignment. *Nucleic Acids Res.* **33**, 511–518.
- 441 [29] Nylander, J., 2004 *MrAIC.pl*. Evolutionary Biology Centre, Uppsala University: Pro-
442 gram distributed by the author.
- 443 [30] Ronquist, F. & Huelsenbeck, J. P., 2003 MrBayes 3: Bayesian phylogenetic inference
444 under mixed models. *Bioinformatics* **19**, 1572–1574.
- 445 [31] Stamatakis, A. & Ott, M., 2008 Efficient computation of the phylogenetic likelihood
446 function on multi-gene alignments and multi-core architectures. *Philos. Trans. R. Soc.*
447 *Lond., B, Biol. Sci.* **363**, 3977–3984.
- 448 [32] Kubatko, L. & Degnan, J., 2007 Inconsistency of phylogenetic estimates from concate-
449 nated data under coalescence. *Syst. Biol.* **56**, 17–24.
- 450 [33] Edwards, S., Liu, L. & Pearl, D., 2007 High-resolution species trees without concatena-
451 tion. *Proc. Natl. Acad. Sci. U.S.A.* **104**, 5936–5941.
- 452 [34] Edwards, S., 2009 Is a new and general theory of molecular systematics emerging?
453 *Evolution* **63**, 1–19.
- 454 [35] Bayzid, M. S. & Warnow, T., 2012 Estimating optimal species trees from incomplete
455 gene trees under deep coalescence. *J. Comput. Biol.* **19**, 591–605.

- 456 [36] Castillo-Ramrez, S., Liu, L., Pearl, D., Edwards, S., Knowles, L. & Kubatko, L., 2010
457 Bayesian estimation of species trees: A practical guide to optimal sampling and analy-
458 sis. In *Estimating species trees: Practical and theoretical aspects*, pp. 15–33. Hoboken:
459 Wiley-Blackwell.
- 460 [37] Guindon, S., Dufayard, J.-F., Lefort, V., Anisimova, M., Hordijk, W. & Gascuel, O.,
461 2010 New algorithms and methods to estimate maximum-likelihood phylogenies: As-
462 sessing the performance of PhyML 3.0. *Syst. Biol.* **59**, 307–321.
- 463 [38] Liu, L., Yu, L., Kubatko, L., Pearl, D. K. & Edwards, S. V., 2009 Coalescent methods
464 for estimating phylogenetic trees. *Mol. Phylogenet. Evol.* **53**, 320–328.
- 465 [39] Liu, L., Yu, L., Pearl, D. K. & Edwards, S. V., 2009 Estimating species phylogenies
466 using coalescence times among sequences. *Syst. Biol.* **58**, 468–477.
- 467 [40] Liu, L. & Yu, L., 2010 Phybase: an R package for species tree analysis. *Bioinformatics*
468 **26**, 962–963.
- 469 [41] Seo, T.-K., 2008 Calculating bootstrap probabilities of phylogeny using multilocus se-
470 quence data. *Mol. Biol. and Evol.* **25**, 960–971.
- 471 [42] Hurley, I., Mueller, R., Dunn, K., Schmidt, E., Friedman, M., Ho, R., Prince, V., Yang,
472 Z., Thomas, M. & Coates, M., 2007 A new time-scale for ray-finned fish evolution. *Proc.*
473 *R. Soc. London, Ser. B* **274**, 489–498.
- 474 [43] Santini, F., Harmon, L., Carnevale, G. & Alfaro, M., 2009 Did genome duplication drive
475 the origin of teleosts? A comparative study of diversification in ray-finned fishes. *BMC*
476 *Evol. Biol.* **9**, 194.
- 477 [44] Drummond, A. & Rambaut, A., 2007 BEAST: Bayesian evolutionary analysis by sam-
478 pling trees. *BMC Evol. Biol.* **7**, 214.

- 479 [45] Li, C., Lu, G. & Orti, G., 2008 Optimal data partitioning and a test case for ray-finned
480 fishes (Actinopterygii) based on ten nuclear loci. *Syst. Biol.* **57**, 519–539.
- 481 [46] Inoue, J. G., Miya, M., Tsukamoto, K. & Nishida, M., 2003 Basal actinopterygian
482 relationships: A mitogenomic perspective on the phylogeny of the “ancient fish”. *Mol.*
483 *Phylogenet. Evol.* **26**, 110–120.
- 484 [47] Venkatesh, B., Erdmann, M. & Brenner, S., 2001 Molecular synapomorphies resolve
485 evolutionary relationships of extant jawed vertebrates. *Proc. Natl. Acad. Sci. U.S.A.*
486 **98**, 11382–11387.
- 487 [48] Mabuchi, K., Miya, M., Azuma, Y. & Nishida, M., 2007 Independent evolution of the
488 specialized pharyngeal jaw apparatus in cichlid and labrid fishes. *BMC Evol. Biol.* **7**,
489 10.
- 490 [49] Wainwright, P., Smith, W. & Price, S., *In Press* The evolution of pharyngognathy: A
491 phylogenetic and functional appraisal of the pharyngeal jaw key innovation in labroid
492 fishes and beyond. *Syst. Biol.* .
- 493 [50] Smith, W. & Wheeler, W., 2006 Venom evolution widespread in fishes: A phylogenetic
494 road map for the bioprospecting of piscine venoms. *J. Hered.* **97**, 206–217.
- 495 [51] Smith, W. & Craig, M., 2007 Casting the percomorph net widely: The importance of
496 broad taxonomic sampling in the search for the placement of serranid and percid fishes.
497 *Copeia* **1**, 35–55.
- 498 [52] Dettai, A. & Lecointre, G., 2005 Further support for the clades obtained by multiple
499 molecular phylogenies in the acanthomorph bush. *C. R. Biol.* **328**, 674–689.
- 500 [53] Meynard, C. N., Mouillot, D., Mouquet, N. & Douzery, E. J. P., 2012 A phylogenetic
501 perspective on the evolution of mediterranean teleost fishes. *PLoS ONE* **7**, e36443.
502 (doi:10.1371/journal.pone.0036443).

- 503 [54] Near, T., Meylan, P. & Shaffer, H., 2005 Assessing concordance of fossil calibration
504 points in molecular clock studies: An example using turtles. *Am. Nat.* **165**, 137–146.
- 505 [55] Johnson, G., Ida, H., Sakaue, J., Sado, T., Asahida, T. & Miya, M., 2012 A “living
506 fossil” eel (Anguilliformes: Protanguillidae, fam. nov.) from an undersea cave in Palau.
507 *Proc. R. Soc. Lond., B, Biol. Sci.* **279**, 934–943.
- 508 [56] Janvier, P., 1996 The dawn of the vertebrates: Characters versus common ascent in the
509 rise of current vertebrate phylogenies. *Palaeontology* **39**, 259–287.
- 510 [57] Patterson, C., 1993 Osteichthyes: Teleostei. In *The Fossil Record 2* (ed. M. Benton),
511 pp. 621–656. London: Chapman & Hall.
- 512 [58] Santini, F. & Tyler, J. C., 2003 A phylogeny of the families of fossil and extant
513 tetraodontiform fishes (Acanthomorpha, Tetraodontiformes), Upper Cretaceous to re-
514 cent. *Zool. J. Linn. Soc.* **139**, 565–617.

515 Description of timetree calibration points

516 We assigned fossil calibrations to 14 nodes of the maximum likelihood phylogeny (Fig. 2)
517 to enable divergence time estimation using BEAST v1.72. Below, we justify the bounds for
518 each calibration point.

519 MRCA of Actinopterygii

520 **Fig. 2, node 1; uniform calibration = 392-472 Ma**

521 We used the stegotrachelids fossils from the Givetian/Eifelian boundary (≈ 392 Ma)
522 used by [42] to date the minimum age of the root and assumed an upper bound of
523 472 Ma based upon the minimum age for the split between acanthodians and all other
524 bony fishes [56].

525 MRCA of Actinopteri

526 **Fig. 2, node 2, exponential calibration lower bound = 345 Ma, upper 95%**
527 **= 392 Ma**

528 The oldest fossil belonging to this clade is *Cosmoptycius* from the Tournasian (Car-
529 boniferous, 359-345 Ma) [42]. We used the stegotrachelids fossils from the Give-
530 tian/Eifelian boundary (≈ 392 Ma) used by [42] to date the crown actinopterygians to
531 set the upper bound.

532 MRCA of Holostei

533 **Fig. 2, node 3; exponential calibration lower bound = 284 Ma, upper 95%**
534 **= 345 Ma**

535 The oldest fossil assigned to this clade is the neopterygian *Brachydegma caelatum*,
536 from the Artkinsian (early Permian, 284 Ma) [42]. We used *Cosmoptychius* from the
537 Tournasian (Carboniferous, 359-345 Ma) to set the upper bound [42].

538 MRCA of Teleostei (Fig. 2, node 5; unconstrained)

539 The oldest crown teleost is *Anaethalion*, from the late Kimmeridgian (Jurassic, 152 Ma)

540 [43]. However, due to the appearance of fossils from several major teleost groups (e.g.,
541 the ostarioclupeomorph *Tischlingerichthys viohli*, the euteleost *Leptolepides spratti-*
542 *formis*) in deposits of the same age it seems likely that teleosts arose considerably
543 earlier. We left this node unconstrained in our analysis to obtain an estimate based
544 upon other actionpterygian calibrations and the UCE sequence data.

545 MRCA of Osteoglossomorpha

546 **Fig. 2, node 13; lower bound = 112 Ma, upper 95% = 225 Ma**

547 The oldest taxon assigned to our osteoglossomorph clade (which only includes a sub-
548 set of the major osteoglossomorph lineages) is the arapamid *Laeliichthys ancestralis*
549 from the Aptian Areado Formation of Brazil (Cretaceous, 112 Ma) [57]. We used the
550 Hiodontidae *Yanbiania wangqingica* from the Barremian (Cretaceous, 130 Ma) to set
551 the upper boundary [43].

552 MRCA of Ostarioclupeomorpha

553 **Fig. 2, node 8; lower bound = 149 Ma, upper 95% = 225 Ma**

554 The oldest taxon assigned to this clade is *Tischlingerichthys viohli*, from the upper
555 Tithonian (Jurassic, 149 Ma) [43]. We used the stem teleost *Pholidophorettes salvus*
556 (Pholidophoridae), from the early Carnian/Julian (Triassic, 228-225 Ma) to set the
557 upper bound [43].

558 MRCA of Euteleostei

559 **Fig. 2, node 9, lower bound = 152 Ma, upper 95% = 225 Ma**

560 The oldest taxon assigned to this clade is *Leptolepides sprattiformis* (Orthogonikle-
561 thridae) from the late Kimmeridgian (Jurassic, 152 Ma) [43]. We used the stem teleost
562 *Pholidophorettes salvus* (Pholidophoridae), from the early Carnian/Julian (Triassic,
563 228-225 Ma) to set the upper bound [43].

564 MRCA of Elopomorpha

565 **Fig. 2, node 10, lower bound = 135 Ma, upper 95% = 225 Ma**

566 The oldest taxon assigned to this clade is the albulid *Albuloideorum ventralis*, from
567 the early Hauterivian (Jurassic/Cretaceous border, 135 Ma) [43]. The oldest stem
568 elopomorph is *Anaethalion*, from the late Kimmeridgian (Jurassic, 152 Ma) [43].

569 Characiformes vs Cypriniformes

570 **Fig. 2, node 16, lower bound = 100 Ma, upper 95% = 149 Ma**

571 The oldest taxon assigned to this clade is the characiform *Santanichthys diasii* from
572 the Albian (Cretaceous, 112-100 Ma) [43]. We used *Tischlingerichthys vlohli*, from the
573 upper Tithonian (Jurassic, 149 Ma) to set the upper bound [43]. Our prior assumed
574 100 My as the minimum age, and 149 Ma for the upper bound.

575 Salmoniformes vs Esociformes

576 **Fig. 2, node 12, lower bound = 125 Ma, upper 95% = 152 Ma**

577 The oldest taxon assigned to this clade is *Helgolandichthys schmidi*, from the early
578 Aptian (early Cretaceous, 125 Ma) [43]. We used *Leptolepides sprattiformis* (Or-
579 thogonikleithridae) from the late Kimmeridgian (Jurassic, 152 Ma) to set the upper
580 bound [43].

581 MRCA of Ctenosquamata

582 **Fig. 2, node 11, lower bound = 122 Ma, upper 95% = 152 Ma**

583 The otoliths assigned to *Acanthomorphorum forcallensis* from the Aptian (Early Cre-
584 taceous, 124-122 Ma) represents the oldest fossils assigned to this clade [43]. We used
585 *Leptolepides sprattiformis* (Orthogonikleithridae) from the late Kimmeridgian (Juras-
586 sic, 152 Ma) to set the upper bound [43].

587 MRCA of Acanthopterygii

588 **Fig. 2, node 15, lower bound = 99 Ma, upper 95% = 122 Ma**

589 The oldest taxa assigned to this clade are various Beryciformes (e.g., *Hoplopteryx*,
590 *Trachichthyoides*) from the Cenomanian (Late Cretaceous, 99 Ma) [43]. We used the

591 fossil otoliths assigned to "*Acanthomorphum*" *forcallensis* from the Aptian (Early
592 Cretaceous, 124-122 Ma) to set the upper bound [43].

593 *Gasterosteus* vs *Taenianotus*

594 **Fig. 2, node 21, lower bound = 85 Ma, upper 95% = 122 Ma** We used the
595 oldest gasterosteiform, *Gasterorhamphus zuppichinii* from the Santonian (84-85 Ma)
596 to date the minimum age of this split [57]. We used the fossil otoliths assigned to
597 "*Acanthomorphum*" *forcallensis* from the Aptian (Early Cretaceous, 124-122 Ma) to
598 set the upper bound [43].

599 Lophiiforms vs tetraodontiforms

600 **Fig. 2, node 20, lower bound = 85 Ma, upper 95% = 122 Ma**

601 The oldest taxon assigned to this clade is the stem tetraodontiform *Cretatriacanthus*
602 *guidottii* from the Santonian of Nardo (Italy). We chose this taxon to date the min-
603 imum age rather than other, older, stem tetraodontiformes because preliminary re-
604 examination of the relationships of extant and fossil tetraodontiforms (Santini, unpub-
605 lished) casts doubt on their phylogenetic affinities. We used the fossil otoliths assigned
606 to "*Acanthomorphum*" *forcallensis* from the Aptian (Early Cretaceous, 124-122 Ma)
607 to set the upper bound [43].

608 MRCA of Tetraodontidae

609 **Fig. 2, node 23, lower bound = 32 Ma, upper 95% = 50 Ma**

610 The oldest taxon assigned to this clade is *Archaeotetraodon winterbottomi* from the
611 Oligocene of Caucasus (32-35 Ma) [43]. We used the stem tetraodontid *Eotetraodon*
612 *pygmaeus* from the Ypresian (middle Eocene, 50 Ma) to set the upper bound [58].

Figure Legends

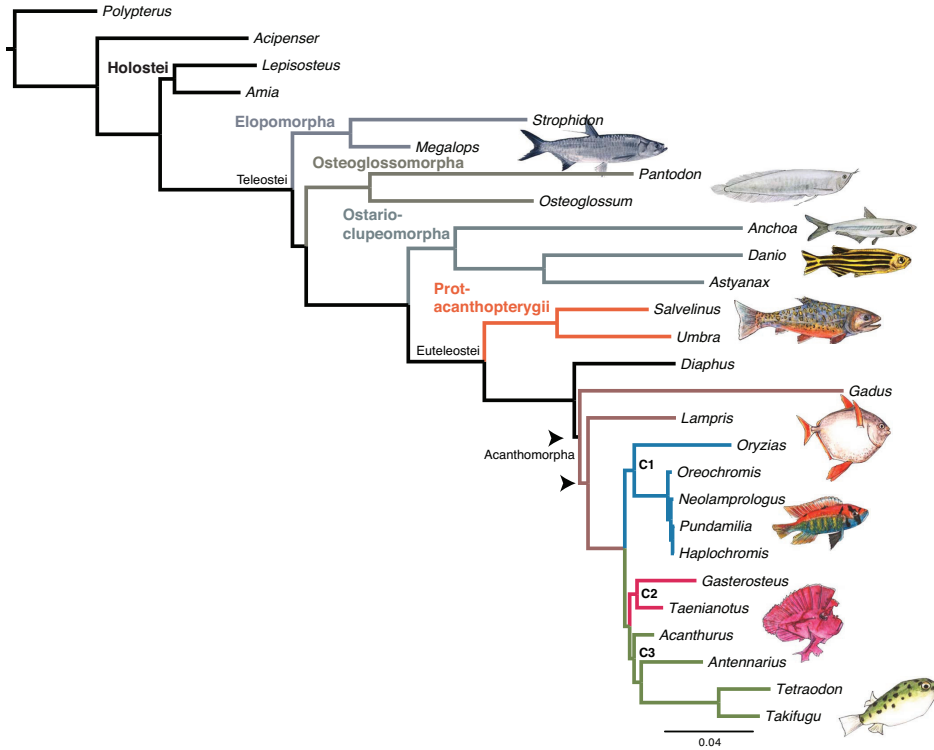


Figure 1. Maximum likelihood phylogram of ray-finned fish relationships based upon UCE sequences. All nodes except for two (indicated by arrows) supported by bootstrap proportions and Bayesian posterior probabilities > 0.99 . Our analysis supports a monophyletic Holostei and reveals the elopomorphs to be the earliest diverging lineage of teleosts. C1, C2, and C3 indicate clades within acanthomorphs consistent with other recent molecular studies (see Discussion).

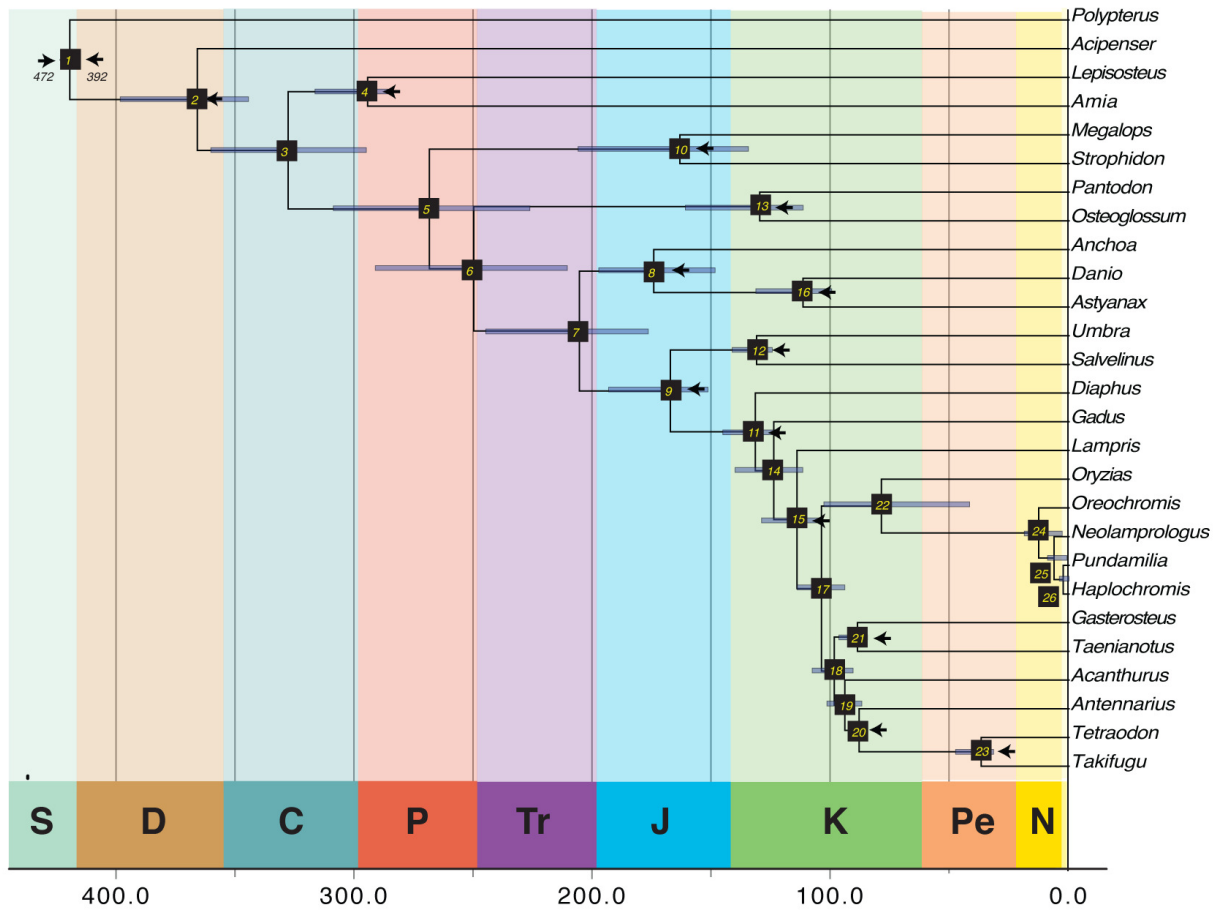


Figure 2. UCE-based timescale of ray-finned fish diversification. Arrows indicate fossil-calibrated nodes (described in Appendix 1). Numbers refer to splits in Fig. 1.

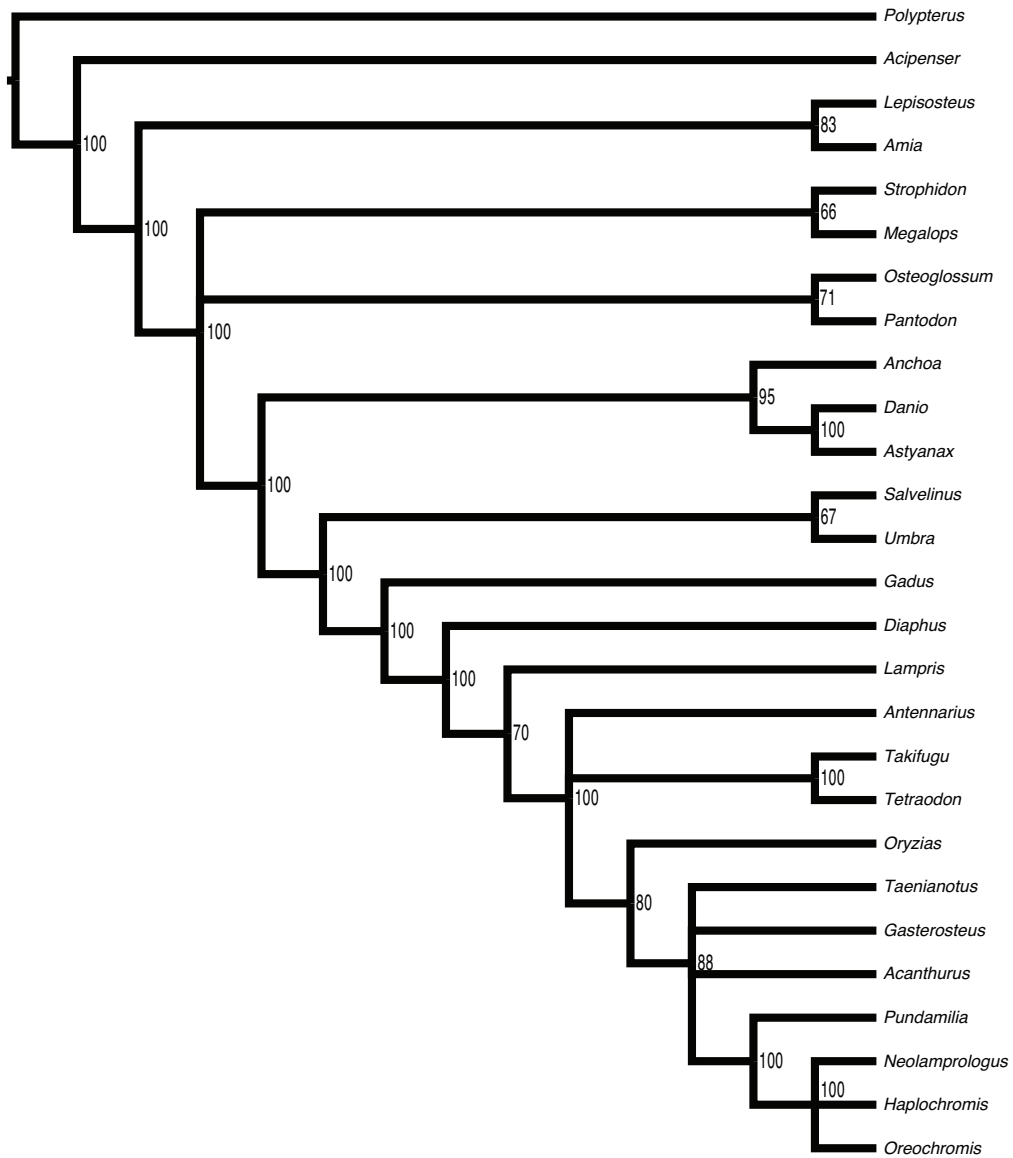


Figure S1. Species tree based upon STAR analysis. Topology based upon analysis of all loci ≥ 50 base pairs that contained both *Polypterus* and *Acipenser* ($N = 136$). Node values indicate bootstrap proportion based upon 1000 replicates. We collapsed nodes having $\leq 50\%$ bootstrap support.

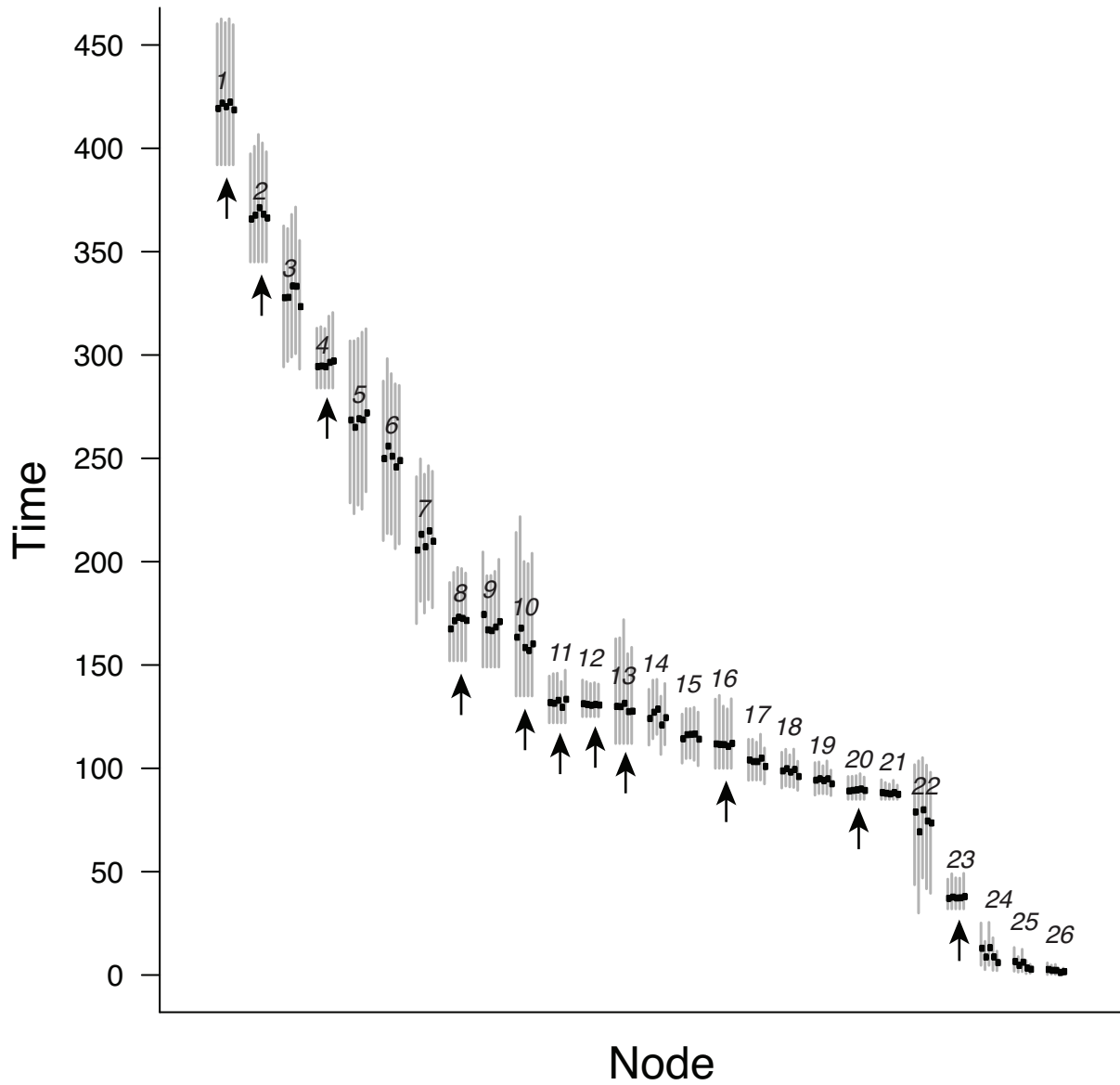


Figure S2. Mean and 95% credible interval of divergence time estimates for subsamples of the UCE data set. Node numbers refer to labels in Fig. 2. Arrows indicate fossil-constrained nodes. For each node, we show the mean and 95% credible interval of five divergence time analyses.

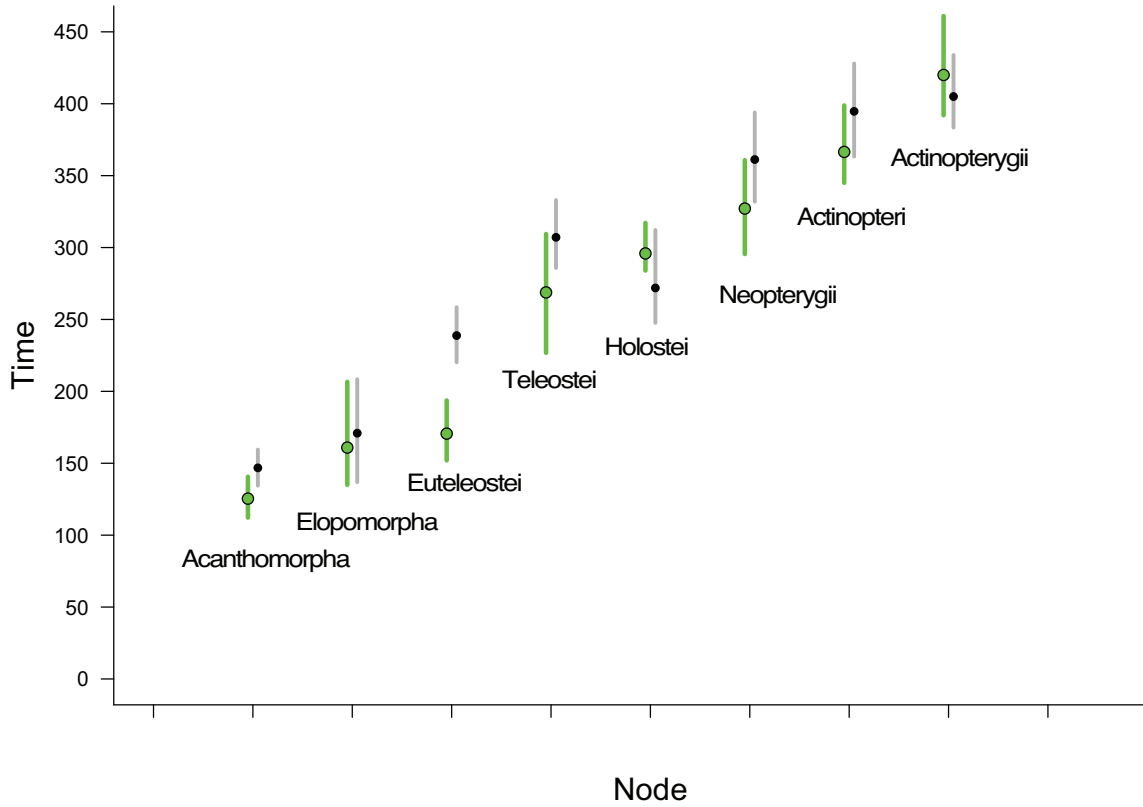


Figure S3. Comparison of ages derived from UCE data and nine nuclear genes [15]. UCE ages are in green. Circles indicate mean age and error bars indicate 95% credible interval.

Tables

Table 1. Divergence times. Node numbers refer to Fig. 2. We averaged mean and 95% credible interval estimates (in Ma) across five subsampled divergence time analyses (see text).

Node	Clade	Split	Age	Min	Max
1	Actinopterygii	<i>Polypterus vs Takifugu</i>	420.0	392.0	461.0
2	Actinopteri	<i>Acipenser vs Takifugu</i>	366.5	345.0	398.8
3	Neopterygii	<i>Lepisosteus vs Takifugu</i>	327.1	295.5	360.8
4	Holostei	<i>Lepisosteus vs Amia</i>	295.9	284.0	317.1
5	Teleostei	<i>Megalops vs Takifugu</i>	268.8	226.8	309.4
6	Osteoglossocephala	<i>Pantodon vs Takifugu</i>	251.7	211.1	291.7
7	Clupeocephala	<i>Anchoa vs Takifugu</i>	210.9	177.1	245.3
8	Ostarioclupeomorpha	<i>Anchoa vs Astyanax</i>	169.5	149.0	197.8
9	Euteleostei	<i>Umbra vs Takifugu</i>	170.6	152.0	193.7
10	Elopomorpha	<i>Megalops vs Strophidon</i>	160.9	135.0	206.6
11	Ctenosquamata	<i>Diaphus vs Takifugu</i>	132.1	122.0	145.8
12	protacanthopterygii	<i>Umbra vs Salvelinus</i>	130.9	125.0	141.8
13	Osteoglossiformes	<i>Pantodon vs Osteoglossum</i>	128.9	112.0	161.5
14	Acanthomorpha	<i>Gadus vs Takifugu</i>	125.4	112.2	140.6
15	–	<i>Lampris vs Takifugu</i>	116.4	104.0	129.5
16	Ostariophysans	<i>Danio vs Astyanax</i>	111.4	100.0	131.9
17	–	<i>Oryzias vs Takifugu</i>	104.1	94.5	114.6
18	–	<i>Gasterosteus vs Takifugu</i>	99.1	91.0	108.2
19	–	<i>Acanthurus vs Takifugu</i>	94.1	87.4	102.0
20	–	<i>Gasterosteus vs Taenianotus</i>	89.7	85.0	97.0
21	–	<i>Antennarius vs Takifugu</i>	87.9	85.0	93.1
22	–	<i>Oryzias vs Haplochromis</i>	76.7	42.1	103.3
23	Tetraodontidae	<i>Tetraodon vs Takifugu</i>	37.5	32.0	48.0
24	Cichlidae	<i>Oreochromis vs Haplochromis</i>	9.9	3.2	19.2
25	–	<i>Neolamprologus vs Haplochromis</i>	4.7	1.3	9.4
26	–	<i>Pundamilia vs Haplochromis</i>	2.0	0.3	4.4

Table 2. Sequence read and assembly statistics for fish species used in this study.

Scientific name	Common name	Number of trimmed reads	Contigs assembled	Reads in contigs	UCE contigs	Reads in UCE contigs	Avg. size	Avg. coverage	Contigs on target	Reads on target
<i>Umbra limi</i>	central mudminnow	2,727,071	1109	740,079	409	564,715	508.8	267.4	0.37	0.21
<i>Diaphus theta</i>	California headlightfish	2,626,413	584	688,635	401	604,295	502.4	299.1	0.69	0.23
<i>Antennarius striatus</i>	striated frogfish	3,724,320	474	2,462,193	418	2,310,186	649.7	850.2	0.88	0.62
<i>Megalops</i> sp.	tarpon	2,771,805	786	650,577	247	231,314	485.4	191.5	0.31	0.08
<i>Astyanax fasciatus</i>	banded astyanax	2,731,668	543	1,444,767	355	1,211,903	526.2	657.2	0.65	0.44
<i>Acanthurus japonicus</i>	Japan surgeonfish	2,017,174	613	1,242,932	454	1,125,871	600.8	405.9	0.74	0.56
<i>Amia calva</i>	bowfin	2,619,643	562	1,608,614	366	1,368,091	578.9	646	0.65	0.52
<i>Lampris guttatus</i>	opah	2,472,439	486	1,350,852	418	1,237,650	568.7	520.2	0.86	0.50
<i>Acipenser fulvescens</i>	lake sturgeon	3,083,152	577	1,129,829	167	467,414	426.9	665.4	0.29	0.15
<i>Anchoa compressa</i>	deep body anchovy	2,617,717	533	783,323	287	625,862	448.6	479.2	0.54	0.24
<i>Danio rerio</i>	zebrafish	2,777,132	518	1,367,065	382	1,166,020	463.4	657.1	0.74	0.42
<i>Polypterus senegalus</i>	gray bichir	3,206,418	576	873,104	294	726,100	557.6	440	0.51	0.23
<i>Pantodon buchholzi</i>	freshwater butterflyfish	3,329,691	466	2,058,929	272	1,399,286	550.4	930.5	0.58	0.42
<i>Strophodon sathete</i>	slender giant moray	3,159,269	1007	448,390	277	246,758	510.6	172.9	0.28	0.08
<i>Osteoglossum bicirrhosum</i>	silver arawana	2,735,138	643	1,565,346	276	813,175	467	623.9	0.43	0.30
<i>Salvelinus fontinalis</i>	brook trout	2,466,696	1118	688,684	166	161,214	408.7	234.8	0.15	0.07
<i>Taenianotus triacanthus</i>	leaf scorpionfish	3,245,453	712	1,423,244	447	1,252,564	652.5	431.4	0.63	0.39